Available online at www.sciencedirect.com
SCIENCE DIRECT®
Journal of Crystal Growth 268 (2004) 536–542
JOURNAL OF CRYSTAL GROWTH
www.elsevier.com/locate/jcrysgro

Laser spectroscopy of epitaxial manganese and zinc fluoride films on silicon

S.V. Gastev[a], K.R. Hoffman[b], A.K. Kaveev[a], R.J. Reeves[c], N.S. Sokolov[a,*]

[a] *Solid State Optics Department, A.F. Ioffe Physico-Technical Institute, Russian Academy of Sciences, 26 Polytekhnicheskaya Str., St. Petersburg 194021, Russia*
[b] *Department of Physics, Whitman College, Walla Walla, WA 99362, USA*
[c] *Department of Physics and Astronomy, University of Canterbury, PB 4800, Christchurch, New Zealand*

Abstract

Laser spectroscopy technique has been applied for studies of MnF_2 and ZnF_2 layers grown by molecular beam epitaxy on silicon substrates with the use of CaF_2 buffer layer. The films were doped during the growth with samarium either from SmF_3 molecular or Sm atomic beams. The excitation wavelength was scanned in the region of $^6H_{5/2} \rightarrow {}^4G_{5/2}$ transitions of Sm^{3+} as well as near the absorption edge of the Mn^{2+} 3d excitons of the tetragonal and orthorhombic phases of MnF_2. The observed emission lines have been assigned to two types of (Sm^{3+}–F^-) centers in the orthorhombic phase and one in the tetragonal rutile phase of MnF_2. Efficient energy transfer from the host lattice to Sm^{3+} centers was observed during excitation into the lowest Mn^{2+} absorption band. Similar centers were also found in ZnF_2 epitaxial films, where along with (Sm^{3+}–F^-) pair centers, an isolated Sm^{3+} center with remote charge compensation was observed. Thus it was shown that Sm^{3+} ions can be used as efficient luminescent probe for characterization of crystal phase composition in the films as well as the local environment of the dopants.

PACS: 32.80.−t; 68.55.Nq; 71.35.AA; 78.66.Nk

Keywords: A1. Characterization; A1. Impurities; A3. Molecular beam epitaxy; B1. Fluorides; B1. Sm^{3+} ions; B2. Dielectric materials

1. Introduction

Recent advances in microelectronics and spintronics stimulated search for new materials with desired optical and magnetic properties. It is well known that manganese fluoride (MnF_2) is a classic antiferromagnetic crystal with well-studied magnetic and optical properties [1]. Zinc fluoride (ZnF_2) is also an insulating wide band gap crystal; however after doping by rare-earth atoms it becomes an n-type semiconductor. It has been recently demonstrated that this material is attractive for applications as efficient light emitter in the UV [2]. Both MnF_2 and ZnF_2 at normal conditions have the rutile type tetragonal crystal

*Corresponding author. Tel.: +7-812-247-6411; fax: +7-812-247-1017.
E-mail address: nsokolov@fl.ioffe.rssi.ru (N.S. Sokolov).

0022-0248/$ - see front matter
doi:10.1016/j.jcrysgro.2004.04.087

structure. It was found, however, that at high pressures and temperatures they can transform into the orthorhombic α-PbO_2-type crystal phase [3,4]. Lately, thick MnF_2 and ZnF_2 layers dominated with metastable orthorhombic phase were grown on CaF_2/Si substrates by molecular beam epitaxy (MBE) [5,6].

Intrinsic luminescence due to Mn^{2+} 3d shell excitons, as well as its excitation spectra in epitaxial MnF_2 films, have been recently studied [7]. Rare-earth ions are known to be sensitive luminescent probe for characterization of epitaxial fluoride layers [8]. However preliminary studies of photoluminescence (PL) of Sm-doped MnF_2 and ZnF_2 films showed that the PL spectra are quite complicated [9]. This circumstance did not allow at that time to obtain meaningful information about the crystalline properties of the films as well as the local environment of the Sm ions. It is known that laser spectroscopy is a powerful tool for studies of rare-earth ions in solids, which enables the separation of PL spectra due to individual light emitting centers [10]. In this work, we studied the optical properties of MBE-grown Sm-doped MnF_2 and ZnF_2 films on silicon substrates using laser spectroscopy. Spectroscopic data were analyzed taking into account information obtained from X-ray diffraction (XRD) and atomic force microscopy measurements.

2. Experimental procedure

Manganese and zinc fluoride films were grown on Si(0 0 1) and Si(1 1 1) substrates by MBE at the Ioffe Physico-Technical Institute of the Russian Academy of Sciences. The Shiraki method was used for chemical cleaning of the Si substrates. The remaining thin oxide layer was evaporated under UHV conditions by heating the substrates up to 1250°C for 1–2 min. This procedure produced atomically clean 2×1 Si(0 0 1) or 7×7 Si(1 1 1) surfaces. A calcium fluoride buffer layer as thick as 30–100 nm was deposited before the ZnF_2 or MnF_2 growth. Growth conditions of the buffer layer determined its surface morphology and crystallographic orientation with respect to the silicon substrate.

Calcium fluoride deposition on Si(1 1 1) at 700–800°C resulted in a smooth CaF_2(1 1 1) buffer layer surface. In case of the growth on Si(0 0 1) below 550°C, CaF_2 tended to form an array of uniformly distributed islands of a nearly square shape and with {1 1 1} facets [11]. The (0 0 1) plane in the islands is parallel to the same plane of the substrate. To obtain relatively flat surface, CaF_2 buffer layers were grown at temperature 300–400°C and then were annealed at 900°C for 1 min [12]. Deposition of CaF_2 on Si(0 0 1) substrate heated above 650°C produced grooved and ridged surface morphology with {1 1 1} facets and CaF_2(1 1 0) plane parallel to the interface with Si(0 0 1) [13].

Epitaxial layers of ZnF_2 and MnF_2 were grown at 100–400°C (100–500°C for MnF_2). To provide smoother surface morphology, in some cases low temperature growth was followed by rapid thermal annealing. Doping was carried out with use of SmF_3 or Sm beams provided by separate effusion cell. Concentration of the dopant was measured ex situ using Camebax. The crystal quality of the layers was characterized in situ by reflection high-energy electron diffraction (RHEED) with the electron energy of 15 keV. The films were covered with a few CaF_2 monolayers in order to protect them from the ambient humidity. XRD were carried out on a DRON system with CuK_α (Ni-filter) radiation. The $\theta-2\theta$ curves were measured in symmetrical Bragg geometry in the (20–132°) 2θ range. The surface morphology measurements were carried out using a P4-SPM-MDT atomic-force microscope manufactured by NT-MDT (Zelenograd, Russia). Cantilevers for this microscope were rendered by "Micromash" (Tallinn, Estonia).

The laser spectroscopy measurements reported here combine excitation and PL techniques. They have been carried out in the optical laboratory of the University of Canterbury (New Zealand, Christchurch). The excitation and emission spectra were obtained simultaneously using an argon ion pumped cw tunable dye laser in conjunction with a 0.3 m spectrometer and CCD detector. In the wavelength region of interest the CCD detection spanned a wavelength range of approximately 30 nm. The range was sufficient to observe

transitions from an excited state to all levels of the ground state manifold for the Sm^{3+} ions. All of the measurements were performed at low temperatures in either a helium flow cryostat or a liquid helium immersion dewar.

3. Samples

The main growth conditions of the samples studied in this work as well as results of their X-ray characterisation are listed in Table 1. Electron diffraction patterns measured in situ indicated epitaxial growth of these films. XRD measurements showed that ZnF_2 forms both rutile-type and α-PbO_2-type structural modifications (samples #5176, #5203 and #5206) in comparable parts, while MnF_2 forms mainly the α-PbO_2-type modification. When grown on the CaF_2(0 0 1) surface obtained at 400°C, ZnF_2 and MnF_2 epitaxial layers differ both in XRD and AFM measurements (Fig. 1). MnF_2 epitaxial layers consist mainly of α-PbO_2-type structural modification with (0 1 0) and (1 0 0) orientations of plane parallel to the interface with Si, whereas ZnF_2 forms polymorphous mixture of rutile and α-PbO_2-type modifications, at that only (1 0 0) orientation of plane parallel to interface with Si was observed. The more disordered surface morphology seen in AFM pictures may be also explained with the fact of polymorphism. Simultaneous presence of polymorphous rutile and α-PbO_2 crystal phases is characteristic feature of the ZnF_2(1 0 0) epitaxial layers revealed by XRD measurements. In MnF_2 epitaxial layer grown at the same conditions, the α-PbO_2-type structural modification dominates [5].

4. Results

The PL spectra of a nominally pure MnF_2 and samarium-doped MnF_2 as well as ZnF_2 epitaxial films under Ar^+ laser ($\lambda = 488$ nm) excitation are

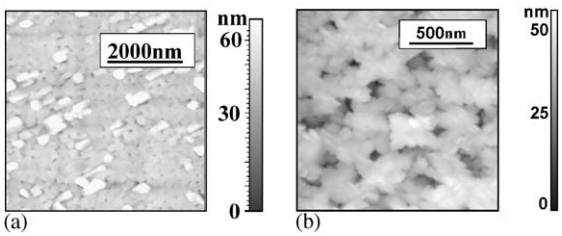

Fig. 1. Surface morphology of epitaxial layers: (a) α-PbO_2-type structural modification of MnF_2 with (1 0 0) and (0 1 0)-planes parallel to interface with Si; and (b) polymorphous mixture rutile + α-PbO_2-type ZnF_2 structural modifications with (1 0 0)-plane parallel to the interface.

Table 1
Growth conditions and results of X-ray characterization of the samples studied in this work

Sample	CaF_2 buffer layer growth temperature/ orientation	Main layer crystalline phase		Sm concentration (mol%)/doping beam
		α-PbO_2	Rutile	
MnF_2 5154	550°C/(0 0 1)-d, (1 1 0)-s	(0 1 0)-e, (1 0 0)-e	(1 0 0)-s	0.2–0.3/SmF_3
MnF_2 5163	770°C/(1 1 0)-d	(1 1 0)-d, (2 2 1) and (1 0 0)-s	(1 0 0)-s	~1/Sm
MnF_2 5167	330°C/(0 0 1)-d	(1 0 0)-d	Was not observed	~1/Sm
ZnF_2 5170	800°C/(1 1 0)-d	(1 1 0)-d, (1 0 0)-s	(1 1 0) and (1 0 0)-s	~1/Sm
ZnF_2 5176	400°C/(0 0 1)-d	(1 0 0)-e	(1 0 0)-e	0.2–0.4/Sm
ZnF_2 5203	400°C/(0 0 1)-d, (1 1 1)-s	(1 0 0)-e	(1 0 0)-e	~1/SmF_3
ZnF_2 5206	800°C/(1 1 0)-d, (1 1 1) and (0 0 1)-s	(1 0 0)-e	(1 0 0)-e, (1 1 0)-s	0.2–0.3/SmF_3
ZnF_2 5207	400°C/(0 0 1)-d	(1 0 0)-d, (0 0 1)-s	(1 0 0)-s	0.2–0.3/SmF_3

d—dominant, e—essential and s—small part of the layer.

shown in Fig. 2. One can see that a broad phonon assisted side band at 575 nm dominates in the pure MnF_2 film while sharp and intense Sm^{3+} peaks are observed in the MnF_2:Sm sample. The energy diagram for Mn^{2+} exciton and Sm^{3+} ion levels is shown in Fig. 3. It is noteworthy that the exciton energy is just a little bit higher than that of the $^4G_{5/2}$ Sm^{3+} manifold. Apparently 488 nm argon laser irradiation may result in both generation of Mn^{2+} excitons and direct excitation of Sm^{3+} ions. The ZnF_2 matrix has no absorption bands in the visible region and the Sm^{3+} PL in this film can be only caused by the direct excitation of samarium via the $^6H_{5/2} \rightarrow {}^4F_{5/2}$ optical transition, which energy is near to the laser photon one. In addition to the $^4G_{5/2} \rightarrow {}^6H_J$ ($J = 5/2$, 7/2, 9/2 and 11/2) transitions, the ZnF_2:Sm film exhibits the $^4F_{3/2} \rightarrow {}^6H_{5/2}$ PL transition, which is not observed in the MnF_2:Sm film (see Fig. 2). This fact confirms an important role of MnF_2 matrix in excitation of Sm^{3+} centers and efficient energy transfer from the host lattice to the impurity centers. The energy transfer mechanisms were early discussed in Ref. [14] for Eu^{3+} and Er^{3+} ions in MnF_2 bulk crystals.

All the transitions show more peaks than are expected at helium temperature for one simple Sm^{3+} PL center with low symmetry environment: 3, 4, 5 and 6 peaks for $J = 5/2$, 7/2, 9/2 and 11/2, respectively. For example, the $^4G_{5/2} \rightarrow {}^6H_{7/2}$ transition in the MnF_2:Sm film, presented in the inset to Fig. 2 shows eight well pronounced PL peaks instead of four peaks expected for one center. To clarify the complicated character of the Sm^{3+} PL spectra obtained at non-resonant 488 nm excitation, we have measured them at selective excitation spectra in the region of the $^6H_{5/2} \rightarrow {}^4G_{5/2}$ transition. The results obtained for MnF_2 and ZnF_2 films are shown in Figs. 4 and 5, respectively. One can see that MnF_2 and ZnF_2 films show several different Sm^{3+} centers with four peak pattern of the PL spectra. However the PL of MnF_2 under

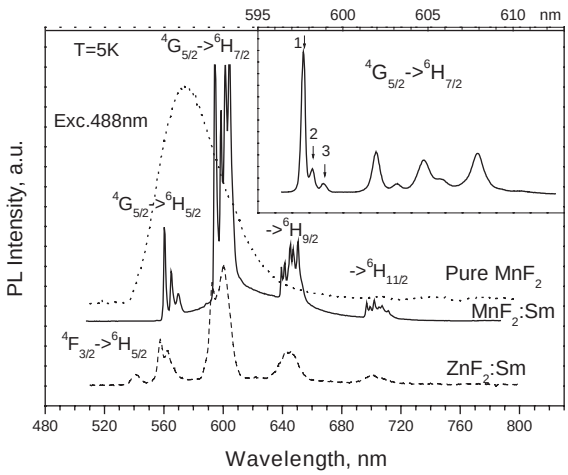

Fig. 2. The PL spectra of the pure (dots), Sm-doped MnF_2 (solid line) and ZnF_2 (dashed curve) films under Ar-laser excitation at 5 K. Inset: Sm^{3+} PL spectrum due to the $^4G_{5/2} \rightarrow {}^6H_{7/2}$ transition in MnF_2:Sm film.

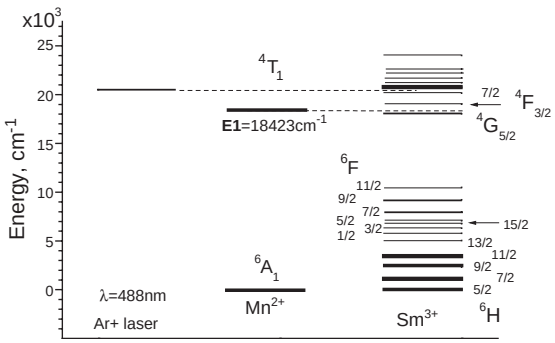

Fig. 3. Energy diagram of the Sm^{3+} ion manifolds compared with laser and E1 exciton energy.

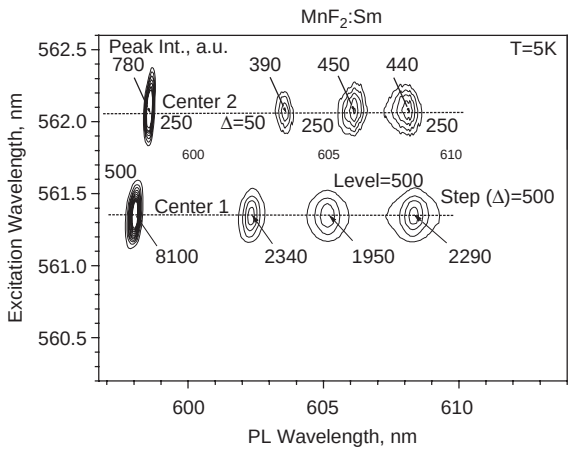

Fig. 4. Equal intensity contour plot of the PL caused by Sm^{3+} ions in MnF_2:Sm (#5154) at the direct excitation of the $^6H_{5/2} \rightarrow {}^4G_{5/2}$ transition.

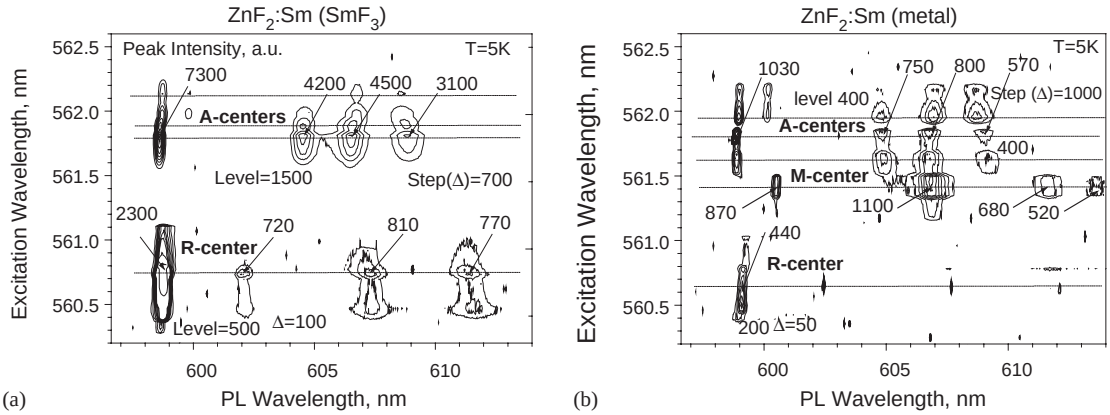

Fig. 5. Equal intensity contour plots of the PL caused by Sm^{3+} ions in ZnF_2:Sm doped from SmF_3 (#5207) (a) and Sm beams (#5176) (b) at direct excitation of the $^6H_{5/2} \rightarrow {}^4G_{5/2}$ transition.

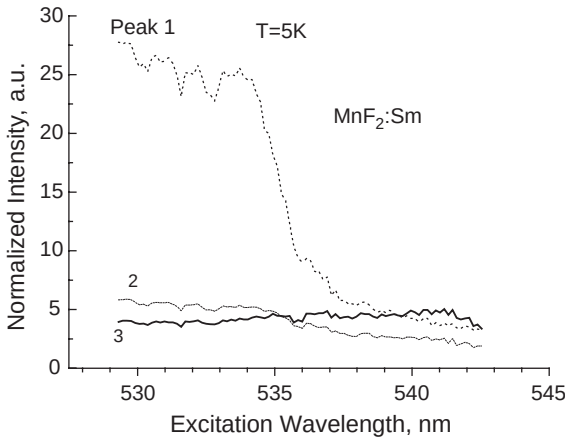

Fig. 6. The normalized on MnF_2 broad band PL intensity at 620 nm excitation spectra of three short wavelength peaks from the inset to Fig. 2 (labeled there as 1, 2 and 3) in the area of the MnF_2 film intrinsic absorption (#5154).

non-resonant excitation shown in the inset to Fig. 2 cannot be understood taking into account only the contributions of the centers 1 and 2 clearly seen at the selective excitation conditions presented in Fig. 4. It looks that the weaker short wavelength peak (3) in the inset has some other origin which will be discussed in more detail below.

The normalized excitation spectra of three short wavelength peaks from the inset to Fig. 2 (labeled there as 1, 2 and 3) are shown in Fig. 6. One can see in Fig. 2 that the MnF_2:Sm film spectrum (solid curve) shows the Sm^{3+} PL narrow peaks and the broad band with maximum near 610 nm. This band is due to the PL of the MnF_2 matrix including its major orthorhombic and minor rutile constituents. The PL intensity is proportional to the light absorption in the MnF_2 film. The intensity of Sm^{3+} PL peaks depends on the energy transfer mechanisms from the matrix to the ions. Therefore, the division of the Sm^{3+} peak intensity to the PL intensity of the matrix follows the efficiency of the Sm^{3+} PL center per one photon absorbed by matrix, or the quantum yield of the PL center.

We used here the matrix PL intensity at 620 nm because it is near maximum and just between $^4G_{5/2} \rightarrow {}^6H_{7/2}$ and $^4G_{5/2} \rightarrow {}^6H_{9/2}$ optical transitions. Because the absorption band of the orthorhombic and rutile components of MnF_2:Sm film starts at difference wavelength, the quantum yield spectra show more distinct the relation of the PL lines belonging to Sm^{3+} ions with local crystal structure of the MnF_2 film. Moreover, these spectra have better signal to noise ratio because mentioned above normalization procedure drastically reduces the noise arising from some fluctuations of the excitation light intensity. It is seen that the spectra for peaks 1 and 2 are quite similar and have well pronounced threshold near 537 nm but the spectrum corresponding to peak 3 is different and has a maximum near 541 nm. Using selective excitation at 541 nm we could separate the

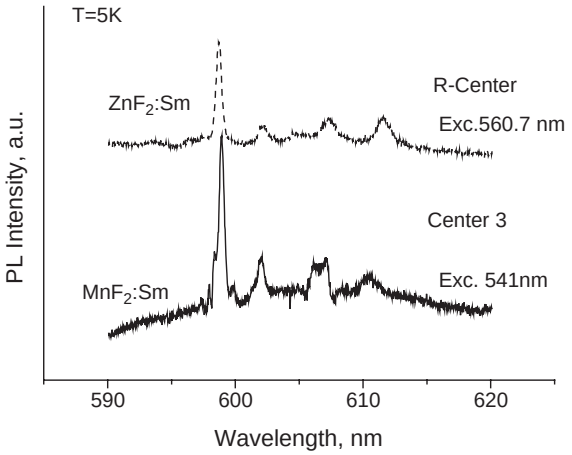

Fig. 7. The Sm^{3+} PL spectra in ZnF_2 (#5207) at 560.7 nm (R-center) and in MnF_2 (#5154) at 541 nm (Center 3) excitation light wavelength.

relatively weak additional Sm^{3+} center having PL spectrum shown in the lower part of Fig. 7. PL spectrum of the R-center in ZnF_2 film (see Figs. 5a and b) is shown at the upper part of Fig. 7. One can see that both spectra look very similar indicating the same nature of the centers.

A new PL center was found in the ZnF_2 films doped with Sm from a Sm atomic beam. In Fig. 5b, in addition to A-center and weak R-centers a new strong M-center appears. It is natural to expect that this center can be due to lack of fluorine ions providing charge compensation for Sm^{3+} ions substituting Zn^{2+} in the lattice. In case of MnF_2 films doped from a Sm atomic beam no centers specific to such type of doping were observed.

5. Discussion

It is known from XRD measurements that epitaxial MnF_2 films grow on silicon substrates in the orthorhombic α-PbO_2-type crystal phase [5]. However in some films a weak admixture of the rutile tetragonal phase can also be seen. ZnF_2 films on silicon usually contain microcrystals of both mentioned phases. The intrinsic absorption and PL spectra of rutile MnF_2 are well known from bulk crystal studies [1]. Fig. 8 presents such spectra for epitaxial MnF_2 films measured in Ref. [15].

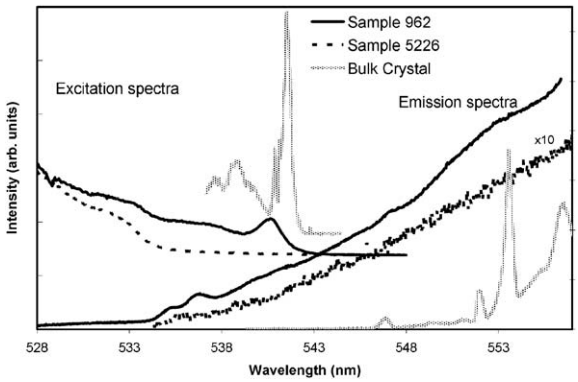

Fig. 8. The emission and excitation spectra at 2 K from two thin films, and a bulk MnF_2 crystal [15].

One can see that the excitation spectrum of the film with α-PbO_2-type crystal structure (#5226) has a short wavelength shift compared to the rutile bulk crystals; this is consistent with PL spectra of the films. But some films demonstrate the absorption in 534–543 nm range with a maximum at 541 nm (#962). This indicates presence of the microcrystals with the rutile structure in such films.

Therefore we can conclude that the PL spectrum of the MnF_2:Sm film at 541 nm excitation (Fig. 7) is related with Sm^{3+} ions in the rutile microcrystals (Center 3). The similarity of the excitation spectra of the centers 1 and 2 (Fig. 6) with absorption of the orthorhombic phase (Fig. 8) allows us to relate these centers with α-PbO_2 phase of the MnF_2 film. Replacement of Mn^{2+} ions by Zn^{2+} ones in the same crystal structure should not have much influence on the Sm^{3+} PL spectra because the $^4G_{5/2} \rightarrow {}^6H_J$ transitions occur inside the 4f shielded shell. Indeed, the spectra of the R- and A-centers in ZnF_2 films look very similar with the center 3 and the centers 1and 2 in MnF_2 films, respectively (see Figs. 4, 5 and 7). Therefore it is quite obvious that A-centers are related to the α-PbO_2-type crystal phase and the R-center is associated with the rutile phase in the ZnF_2 films.

It is well known that for trivalent dopants substituting divalent metals of the host lattice in ionic crystals, extra positive charge compensation is needed. For the films doped from SmF_3 molecular beam it is expected that charge compensation is provided by interstitial negatively

charged fluorine ion located nearby from Sm^{3+} dopant. This situation was also observed for bulk CaF_2 crystals doped with Sm by mixing starting CaF_2 powder with small amount of SmF_3 [16]. In the films doped from a samarium atomic beam some other mechanism of the charge compensation must occur. ZnF_2 (similar to better studied CdF_2) after doping by trivalent ions acquires shallow donor centers resulting in high free electron concentration [17]. One can expect that these electrons can provide necessary extra charge compensation in the ZnF_2 layers doped from Sm beam. This mechanism will result in different crystal field for Sm^{3+} ion and different energy of optical transitions explaining the appearance of M-centers.

6. Conclusion

Applying laser spectroscopy, we succeeded in understanding quite complicated spectra of MnF_2:Sm and ZnF_2:Sm epitaxial films observed at non-resonant excitation. Two Kramers type (Sm^{3+}–F^{-}) pair centers in orthorhombic phase and one in the tetragonal rutile phase of MnF_2 were extracted. Efficient energy transfer to Sm^{3+} centers was observed during excitation into Mn^{2+} lowest absorption band. Similar pair centers were also found in both crystalline phases of the ZnF_2 epitaxial films. It was revealed that doping from samarium atomic beam resulted in formation of the center with different mechanisms of charge compensation. Presumably, this mechanism is related with n-type conductivity earlier observed in doped ZnF_2 crystals. These studies showed that Sm^{3+} ions can be used as efficient luminescent probe for characterization of crystal phase composition in the films as well as the local environment of the dopant.

Acknowledgements

The authors would like to thank Profs. W.M. Yen and A.A. Kaplyanskii for stimulating interest to this work. Support of Russian Foundation for Basic Research (Grants Nos. 02-02-17588 and 03-02-17637), Russian Ministry of Science, the MacDiarmid Institute for Advanced Materials and Nanotechnology (New Zealand) is greatly appreciated.

References

[1] A.H. Morrish, The Physical Principles of Magnetism, Wiley, New York, 1965;
D.D. Sell, J. Appl. Phys. 39 (2) (1968) 1030.
[2] T. Senda, Y. Cho, T. Hirakawa, H. Okamoto, H. Takakura, Y. Hamakawa, Jpn. J. Appl. Phys. 39 part 1, No. 8 (2000) 4716.
[3] L.M. Azzaria, F. Dachille, J. Phys. Chem. 65 (1961) 889.
[4] S.S. Kabalkina, L.F. Vereshchagin, L.M. Lityagina, Sov. Phys. JETP 29 (1969) 803.
[5] A.G. Banshchikov, O.V. Anisimov, N.F. Kartenko, M.M. Moisseeva, N.S. Sokolov, V.P. Ulin, Proceedings of the 9th International Symposium on Nanostructures: Physics and Technology, St. Petersburg, Russia, June 18–22, 2001, p. 25.
[6] A.G. Banshchikov, N.F. Kartenko, A.K. Kaveev, M.M. Moisseeva, N.S. Sokolov, Proceedings of the 10th International Symposium on Nanostructures: Physics and Technology, St. Petersburg, Russia, June 17–21, 2002, p. 22.
[7] R.J. Reeves, X. Wang, W.M. Yen, O.V. Anisimov, A.G. Banshchikov, S.V. Gastev, N.S. Sokolov, J. Lumin. 94-95 (2001) 207;
K.R. Hoffman, R.J. Reeves, O.V. Anisimov, S.V. Gastev, N.S. Sokolov, W.M. Yen, Abstracts of International Conference on Advanced Materials and Nanotechnology (AMN-1), Wellington, 9–14 February, 2003, p. 87.
[8] N.S. Sokolov, N.L. Yakovlev, Proc. SPIE 2706 (1996) 57.
[9] S.V. Gastev, A.K. Kaveev, R.J. Reeves, N.S. Sokolov, Abstracts of International Conference on Advanced Materials and Nanotechnology (AMN-1), Wellington, 9–14 February, 2003, p. 68.
[10] S. Mho, J.C. Wright, J. Chem. Phys. 81 (3) (1984) 1421.
[11] R.W. Fathauer, L.J. Schowalter, Appl. Phys. Lett. 45 (5) (1984) 519.
[12] T. Asano, H. Ishiwara, S. Furukawa, Jpn. J. Appl. Phys. 27 (7) (1988) 1193.
[13] N.S. Sokolov, S.M. Suturin, Thin Solid Films 367 (1/2) (2000) 112.
[14] B.A. Wilson, W.M. Yen, J. Hegarty, G.F. Imbusch, Phys. Rev. B 19 (1979) 4238.
[15] K.R. Hoffman, S.V. Gastev, A.K. Kaveev, N.S. Sokolov, R.J. Reeves, J. Lumin. 108 (1–4) (2004) 25.
[16] J-P.R. Wells, R.J. Reeves, Phys. Rev. B 61 (2000) 13593.
[17] J.H. Crawford Jr., F.E. Williams, J. Chem. Phys. 18 (6) (1950) 775.